Regular Article – Theoretical Physics

Next-to-leading BFKL phenomenology of forward-jet cross sections at HERA

O. Kepka[1,a], C. Marquet[2,b], R. Peschanski[3,4,c], C. Royon[1,d]

[1] IRFU/Service de physique des particules, CEA/Saclay, 91191 Gif-sur-Yvette cedex, France
[2] RIKEN BNL Research Center, Brookhaven National Laboratory, Upton, NY 11973, USA
[3] Institut de physique théorique, CEA/Saclay, 91191 Gif-sur-Yvette cedex, France
[4] URA 2306, unité de recherche associée au CNRS

Abstract. We show that the forward-jet measurements performed at HERA allow for a detailed study of corrections due to next-to-leading logarithms (NLL) in the Balitsky–Fadin–Kuraev–Lipatov (BFKL) approach. While the description of the $d\sigma/dx$ data shows small sensitivity to NLL-BFKL corrections, these can be tested by the triple differential cross section $d^3\sigma/dx\,dk_T^2\,dQ^2$ recently measured. These data can be successfully described using a renormalization-group improved NLL kernel, while the standard next-to-leading-order QCD or leading-logarithm BFKL approaches fail to describe the same data in the whole kinematic range. We present a detailed analysis of the NLL scheme and renormalization-scale dependences and also discuss the photon impact factors.

1 Introduction

Forward-jet production in lepton–proton deep inelastic scattering is a process in which a jet is detected at forward rapidities in the direction of the proton. This process is characterized by two hard scales: Q^2, the virtuality of the intermediate photon that undergoes the hadronic interaction, and k_T^2, the squared transverse momentum of the forward jet. When the total energy of the photon–proton collision W is sufficiently large, corresponding to a small value of the Bjorken variable $x \simeq Q^2/W^2$, forward-jet production is relevant [1] for testing the Balitsky–Fadin–Kuraev–Lipatov (BFKL) approach [2–4].

In fixed-order perturbative QCD calculations, the hard cross section is computed at fixed order with respect to α_s, and large logarithms coming from the strong ordering between the proton scale and the forward-jet scale are resummed using the Dokshitzer–Gribov–Lipatov–Altarelli–Parisi (DGLAP) evolution equation [5–8]. However, in the small-x regime, other large logarithms arise in the hard cross section itself, due to the strong ordering between the energy W and the hard scales. These can be resummed using the BFKL equation, at leading (LL) and next-to-leading (NLL) logarithmic accuracy [2–4, 9–11].

It has been shown that the H1 and ZEUS $d\sigma/dx$ forward-jet data [12–15] are well described by LL-BFKL

predictions [16, 17], while fixed-order perturbative QCD predictions at next-to-leading order (NLOQCD) fail to describe the data, underestimating the cross section by a factor of about 2 at small values of x. However, these tests on the relevance of BFKL dynamics have not been considered fully conclusive. On the theoretical side, it has been found that NLL-BFKL corrections [9–11] could be large enough to invalidate the tests. On the phenomenological side, other models such as DGLAP evolution with a "resolved" photon [18] could increase the NLOQCD predictions and come to reasonable agreement with the data.

The recent experimental forward-jet measurements [12, 13] performed at HERA motivate a new phenomenological analysis of BFKL effects in forward-jet cross sections. In particular, the triple differential cross section $d\sigma/dx\,dk_T^2\,dQ^2$, allows for a detailed study of the QCD dynamics of forward jets. Contrary to the $d\sigma/dx$ data, which were obtained with kinematical cuts such that $r = k_T^2/Q^2 \sim 1$, the triple differential cross section is measured with different sets of cuts such that the data are also sensitive to the regime $r \gg 1$, where the two hard scales of the problem are somewhat ordered. While LL-BFKL predictions describe well the data obtained with $r \sim 1$, it was noticed [17] that they fail to describe the $r \gg 1$ regime, indicating the need for NLL-BFKL corrections.

It was known that NLL-BFKL corrections could be large due to the appearance of spurious singularities in contradiction with renormalization-group requirements. However, it has been realized [19–21] that a renormalization-group improved NLL-BFKL regularization can solve the singularity problem and lead to reasonable NLL-BFKL

[a] e-mail: oldrich.kepka@cea.fr
[b] e-mail: marquet@quark.phy.bnl.gov
[c] e-mail: robi.peschanski@cea.fr
[d] e-mail: christophe.royon@cea.fr

kernels (see also [22–24] for different approaches). This motivates the present phenomenological study of NLL-BFKL effects in forward-jet production. Even though the determination of the next-to-leading impact factors is still in progress [25–27], our analysis allows us to study the NLL-BFKL framework and the remaining ambiguity corresponding to the dependence on the specific regularization scheme. Our goal is to confront the new experimental data, in particular the triple differential cross section, to NLL-BFKL predictions in different schemes.

In [28], such a phenomenological investigation has been devoted to the proton structure function data, taking into account NLL-BFKL effects through an "effective kernel" (introduced in [20, 21]) using different schemes. A saddle-point approximation for hard enough scales was used to evaluate the BFKL Mellin integration, which allowed one to obtain a phenomenological description of NLL-BFKL effects. In the present study, devoted to forward-jet production, we take into account the proper symmetric two-hard-scale feature of the forward-jet problem when introducing the effective kernel, and we implement the NLL-BFKL effects with an exact Mellin integration, rather than a saddle-point approximation.

Some preliminary results, mostly based on the saddle-point approach, were presented in [29]. They showed the potential of forward-jet data on $\mathrm{d}\sigma/\mathrm{d}x$ and specially $\mathrm{d}\sigma/\mathrm{d}x\,\mathrm{d}k_\mathrm{T}^2\,\mathrm{d}Q^2$ to discuss NLL effects in the BFKL approach. In this paper, we systematically use an exact Mellin integration, and we present a detailed analysis of the NLL scheme and scale dependences and also discuss the sensitivity of our NLL-BFKL descriptions with respect to the photon impact factors. We also study the NLOQCD predictions, testing their relevance by comparing the use of different parton densities and different renormalization and factorization scales.

The plan of the paper is the following. In Sect. 2, we present the phenomenological NLL-BFKL formulation of the forward-jet cross section for the two schemes called S3 and S4, while briefly highlighting the principles of its derivation. In Sect. 3, we compare the predictions of the two NLL-BFKL schemes with the data and also with LL-BFKL and NLOQCD predictions. We discuss the dependence of our results on the choice of the hard scale with which α_s is running in Sect. 4, and on the assumption made for the photon impact factors in Sect. 5. Section 6 presents the scale and parton-density dependences of the NLOQCD predictions. Section 7 is devoted to conclusions and an outlook.

2 Forward-jet production in the BFKL framework

Forward-jet production in a lepton–proton collision is represented in Fig. 1 with the different kinematic variables. We denote by $\sqrt{s}$ the total energy of the lepton–proton collision and by Q^2 the virtuality of the intermediate photon that undergoes the hadronic interaction. We shall use the usual kinematic variables of deep inelastic scattering: $x =$
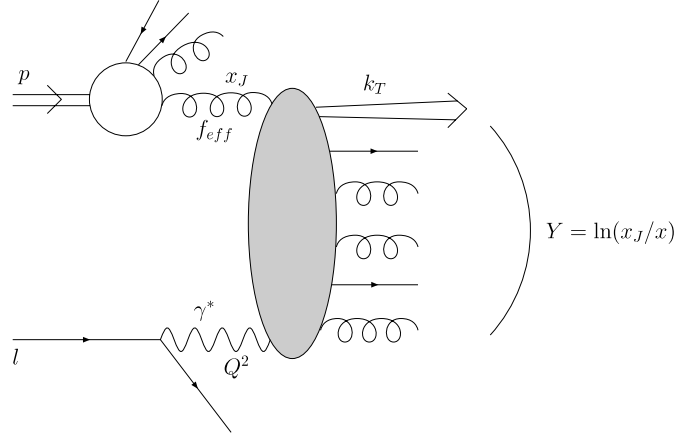

Fig. 1. Production of a forward jet in a lepton–proton collision. The kinematic variables of the problem are displayed. Q^2 is the virtuality of the photon that undergoes the hadronic interaction. k_T is the transverse momentum of the forward jet and x_J is its longitudinal momentum fraction with respect to the incident proton. Y is the (large) rapidity interval between the two hard probes

$Q^2/(Q^2 + W^2)$ and $y = Q^2/(xs)$, where W is the center-of-mass energy of the photon–proton collision. In addition, $k_\mathrm{T} \gg \Lambda_\mathrm{QCD}$ is the transverse momentum of the jet and x_J its longitudinal momentum fraction with respect to the proton. The QCD cross section for forward-jet production reads

$$\frac{\mathrm{d}^{(4)}\sigma}{\mathrm{d}x\,\mathrm{d}Q^2\,\mathrm{d}x_J\,\mathrm{d}k_\mathrm{T}^2} = \frac{\alpha_\mathrm{em}}{\pi x Q^2}$$
$$\times \left\{ \left(1 - y + \frac{y^2}{2}\right) \frac{\mathrm{d}\sigma_\mathrm{T}^{\gamma^*p\to JX}}{\mathrm{d}x_J\,\mathrm{d}k_\mathrm{T}^2} + (1-y)\frac{\mathrm{d}\sigma_\mathrm{L}^{\gamma^*p\to JX}}{\mathrm{d}x_J\,\mathrm{d}k_\mathrm{T}^2} \right\},$$
$$(1)$$

where $\mathrm{d}\sigma_\mathrm{T,L}^{\gamma^*p\to JX}/\mathrm{d}x_J\,\mathrm{d}k_\mathrm{T}^2$ is the cross section for forward-jet production in the collision of the transversely (T) or longitudinally (L) polarized virtual photon with the target proton.

In the following, we consider the high-energy regime $x \ll 1$, in which the rapidity interval $Y = \log(x_J/x)$ is assumed to be very large. The NLL-BFKL forward-jet cross section of our analysis is given by

$$\frac{\mathrm{d}\sigma_\mathrm{T,L}^{\gamma^*p\to JX}}{\mathrm{d}x_J\,\mathrm{d}k_\mathrm{T}^2} = \frac{\alpha_\mathrm{s}(k_\mathrm{T}^2)\alpha_\mathrm{s}(Q^2)}{k_\mathrm{T}^2 Q^2} f_\mathrm{eff}(x_J, k_\mathrm{T}^2)$$
$$\times \int \frac{\mathrm{d}\gamma}{2\pi\mathrm{i}} \left(\frac{Q^2}{k_\mathrm{T}^2}\right)^\gamma \phi_\mathrm{T,L}^\gamma(\gamma)\,\mathrm{e}^{\bar{\alpha}(k_\mathrm{T}Q)\chi_\mathrm{eff}[\gamma,\bar{\alpha}(k_\mathrm{T}Q)]Y}, \quad (2)$$

with the complex integral running along the imaginary axis from $1/2 - \mathrm{i}\infty$ to $1/2 + \mathrm{i}\infty$. The running coupling is given by

$$\bar{\alpha}(k^2) = \alpha_\mathrm{s}(k^2)N_c/\pi = \left[b\log\left(k^2/\Lambda_\mathrm{QCD}^2\right)\right]^{-1},$$
$$b = \frac{11N_c - 2N_f}{12N_c}. \quad (3)$$

In (2), the NLL-BFKL effects are phenomenologically taken into account by the effective kernel $\chi_{\mathrm{eff}}(\gamma, \bar{\alpha})$. Let us now give further details on this approximation.

The scheme-dependent NLL-BFKL kernels provided by the regularization procedure $\chi_{\mathrm{NLL}}(\gamma, \omega)$ depend on γ, the Mellin variable conjugate to Q^2/k_{T}^2 and ω, the Mellin variable conjugate to W^2/Qk_{T}. In this work we shall consider the S3 and S4 schemes [19], recalled in Appendix A, in which χ_{NLL} is supplemented by an explicit $\bar{\alpha}$ dependence. One writes the following *consistency condition* [19, 30, 31]:

$$\omega = \bar{\alpha}\, \chi_{\mathrm{NLL}}\left(\gamma, \omega\right), \tag{4}$$

which represents the diagonalized form of the NLL-BFKL evolution equation and allows one to formulate the cross section (2) in terms of $\chi_{\mathrm{eff}}(\gamma, \bar{\alpha})$. The approximation amounts to introduce the effective kernel to satisfy the consistency condition. Indeed, the effective kernel $\chi_{\mathrm{eff}}(\gamma, \bar{\alpha})$ is defined from the NLL kernel $\chi_{\mathrm{NLL}}(\gamma, \omega)$ by solving the implicit equation

$$\chi_{\mathrm{eff}}(\gamma, \bar{\alpha}) = \chi_{\mathrm{NLL}}\left[\gamma, \bar{\alpha}\chi_{\mathrm{eff}}(\gamma, \bar{\alpha})\right], \tag{5}$$

as a solution of the consistency condition (4).

To highlight how the effective kernel enters in the formulation of the forward-jet cross section, let us consider the following inverse Mellin transformation over ω, the variable conjugate to e^Y ($\sim$ the energy squared), where $I(\gamma, \omega)$ represents next-to-leading order corrections to the LO impact factors ϕ^γ:

$$\int \frac{\mathrm{d}\omega}{2\pi \mathrm{i}} \frac{I(\gamma, \omega)\,\mathrm{e}^{\omega Y}}{\omega - \bar{\alpha}\chi_{\mathrm{NLL}}(\gamma, \omega)}$$
$$= \frac{I[\gamma, \bar{\alpha}\chi_{\mathrm{eff}}(\gamma, \bar{\alpha})]}{1 - \dot{\chi}_{\mathrm{NLL}}[\gamma, \bar{\alpha}\chi_{\mathrm{eff}}(\gamma, \bar{\alpha})]} \mathrm{e}^{\bar{\alpha}\chi_{\mathrm{eff}}(\gamma, \bar{\alpha})Y},$$
$$\dot{\chi}_{\mathrm{NLL}} = \frac{\mathrm{d}\chi_{\mathrm{NLL}}}{\mathrm{d}\omega}. \tag{6}$$

The factor in front of the exponential is an unknown correction, due both to the yet unknown next-to-leading order corrections to the LO impact factors and to the approximations made in satisfying the consistency equation through the effective kernel method. For simplicity, in the γ integration of (2), we choose to factor this term out and treat it as a constant normalization parameter.

Some other comments are in order.

– In (2), the renormalization scale is $k^2 = k_{\mathrm{T}}Q$, in agreement with the energy scale [32]. In practice, one solves (5) with $\bar{\alpha} = \bar{\alpha}(k_{\mathrm{T}}Q)$. Therefore, to each renormalization scale corresponds an effective kernel [28]. In Sect. 4, we shall test the sensitivity of our results when using $k^2 = \lambda\, k_{\mathrm{T}}Q$ and varying λ. Following (5), the effective kernel is modified accordingly for each scheme, and we also modify the energy scale $k_{\mathrm{T}}Q \to \lambda k_{\mathrm{T}}Q$.
– As we pointed out already, in (2) we use the leading-order (Mellin-transformed) impact factors

$$\begin{pmatrix} \phi_{\mathrm{T}}^\gamma(\gamma) \\ \phi_{\mathrm{L}}^\gamma(\gamma) \end{pmatrix} = \pi\alpha_{\mathrm{em}}N_c^2$$
$$\times \sum_q e_q^2 \frac{1}{2\gamma^2} \frac{\Gamma^3(1+\gamma)\Gamma^3(1-\gamma)}{\Gamma(2-2\gamma)\Gamma(2+2\gamma)(3-2\gamma)}$$
$$\times \begin{pmatrix} (1+\gamma)(2-\gamma) \\ 2\gamma(1-\gamma) \end{pmatrix}, \tag{7}$$

for a transversely (T) and longitudinally (L) polarized virtual photon, where e_f is the charge of the quark with flavor f. We consider massless quarks and sum over four flavors in (7). This is justified considering the rather high values of the photon virtuality ($Q^2 > 5\,\mathrm{GeV}^2$) used for the measurement. We point out that our phenomenological approach can be adapted to full NLL accuracy, once the next-to-leading order impact factors are available (the jet impact factors are known at next-to-leading order [33, 34]). For completeness, we shall discuss the sensitivity of our results to typical next-to-leading modifications of $\phi_{\mathrm{T,L}}^\gamma(\gamma)$ in Sect. 5.

– In (2), $f_{\mathrm{eff}}(x_J, k_{\mathrm{T}}^2)$ is the effective parton distribution function and resums the leading logarithms $\log(k_{\mathrm{T}}^2/\Lambda_{\mathrm{QCD}}^2)$. It obeys the following expression:

$$f_{\mathrm{eff}}\left(x_J, k_{\mathrm{T}}^2\right) = g\left(x_J, k_{\mathrm{T}}^2\right)$$
$$+ \frac{C_{\mathrm{F}}}{N_c}\left[q\left(x_J, k_{\mathrm{T}}^2\right) + \bar{q}\left(x_J, k_{\mathrm{T}}^2\right)\right], \tag{8}$$

where g (respectively q, $\bar{q}$) is the gluon (respectively quark, antiquark) distribution function in the incident proton. Since the forward-jet measurement involves perturbative values of k_{T} and moderate values of x_J, (2) features the collinear factorization of f_{eff}, with k_{T}^2 chosen as the factorization scale.

– By comparison, the LL-BFKL formula is formally the same as (2), with the substitutions

$$\chi_{\mathrm{eff}} \to \chi_{\mathrm{LL}}(\gamma) = 2\psi(1) - \psi(1-\gamma) - \psi(\gamma),$$
$$\bar{\alpha}(k^2) \to \bar{\alpha} = \mathrm{const.\ parameter}, \tag{9}$$

where $\psi(\gamma) = \mathrm{d}\log\Gamma(\gamma)/\mathrm{d}\gamma$ is the logarithmic derivative of the Gamma function. One obtains

$$\frac{\mathrm{d}\sigma_{\mathrm{T,L}}^{\gamma^* p \to JX}}{\mathrm{d}x_J\,\mathrm{d}k_{\mathrm{T}}^2} = \frac{\alpha_{\mathrm{s}}(k_{\mathrm{T}}^2)\alpha_{\mathrm{s}}(Q^2)}{k_{\mathrm{T}}^2 Q^2}\, f_{\mathrm{eff}}(x_J, k_{\mathrm{T}}^2)$$
$$\times \int \frac{\mathrm{d}\gamma}{2\pi \mathrm{i}}\left(\frac{Q^2}{k_{\mathrm{T}}^2}\right)^\gamma \phi_{\mathrm{T,L}}^\gamma(\gamma)\, \mathrm{e}^{\bar{\alpha}\chi_{\mathrm{LL}}(\gamma)Y}. \tag{10}$$

Inserting (2) (respectively (10)) into (1) gives the forward-jet cross section in the NLL-BFKL (respectively LL-BFKL) energy regime. In the LL-BFKL case, this is a 2-parameter formula: the overall normalization and $\bar{\alpha}$. In the NLL-BFKL case, each set of scales (Q^2, k_{T}^2) defines the running coupling constant and therefore we deal with only one free parameter, the overall normalization. The interesting property of our phenomenological approach is that (2) has formally the structure of the LL formula, but with only one free parameter and a NLL kernel. The
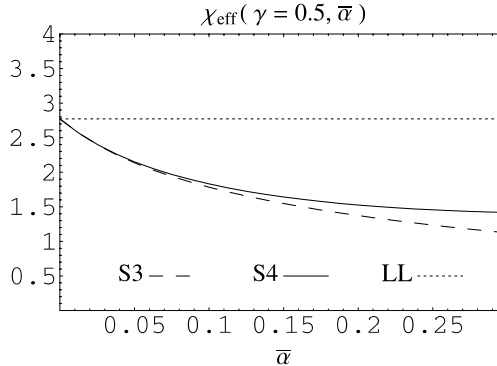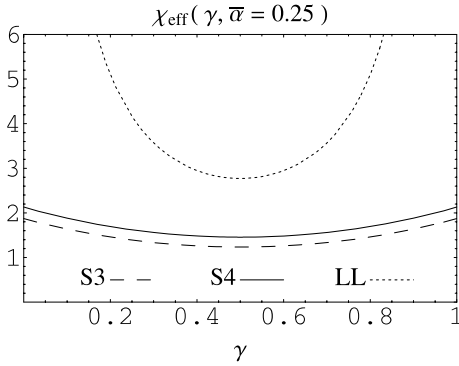
Fig. 2. Comparison between the NLL-BFKL effective kernels $\chi_{\text{eff}}(\gamma, \bar{\alpha})$ obtained by solving the implicit equation (5) in the S3 and S4 schemes. The *left plot* shows $\chi_{\text{eff}}(\gamma, 0.25)$ as a function of γ, while the *right plot* shows the minimum $\chi_{\text{eff}}(0.5, \bar{\alpha})$ as a function of $\bar{\alpha}$. The *dotted curves* show the LL-BFKL kernel $\chi_{\text{LL}}(\gamma)$

delicate aspect of the problem comes from the scheme-dependent effective kernel χ_{eff}. A comparison between the LL-BFKL kernel and the S3 and S4 effective kernels is shown in Fig. 2. As is well known, the NLL modifications to the BFKL kernel are quite important and will play an important phenomenological role in our analysis.

3 NLL description of the H1 data

The NLL-BFKL formula for the fully differential forward-jet cross section is obtained from (1) and (2). To compare the corresponding prediction with the data, one has to carry out a number of integrations over the kinematic variables. They have to be done while properly taking into account the kinematic cuts applied for the different measurements. The procedure is the same as the one described in [17], Appendix A. First one chooses the variables that lead to the weakest possible dependence of the differential cross section (we noticed that the best choice is $1/Q^2$, $1/k_{\text{T}}^2$, $\log(1/x_J)$, and $\log(1/x)$) and then the integrations are computed numerically following the experimental cuts defined in [12, 13].

To fix the normalization (the only free parameter) and check the quality of the data description using the BFKL formalism, we start by fitting the $\mathrm{d}\sigma/\mathrm{d}x$ H1 data [12]. The choice of this data set corresponds to the kinematical domain where the BFKL formalism is expected to hold ($x \ll 1$ and $Q^2/k_{\text{T}}^2 \sim 1$). We then use the relative normalizations obtained between the different NLL BFKL calculations (S3 and S4) to make predictions for the triple differential cross section $\mathrm{d}\sigma/\mathrm{d}x\,\mathrm{d}k_{\text{T}}^2\,\mathrm{d}Q^2$. For this first analysis, the coupling $\bar{\alpha}$ is running with the scale $k_{\text{T}}Q$.

3.1 The cross section $\mathrm{d}\sigma/\mathrm{d}x$

We considered two kinds of fits: the first one is performed using statistical and systematics errors and the second one with statistical errors only. The systematics errors are very much point-to-point correlated, and this is why it is important to perform the fits with statistical errors only. Ideally, one should use the statistical errors added in quadrature with the uncorrelated ones, but this information is not available.

The fit results to the $\mathrm{d}\sigma/\mathrm{d}x$ H1 data are given in Table 1. The χ^2 values (per degree of freedom) of the fits performed using the full (statistical and systematics) errors are quite good, always less than 1, for the two NLL-BFKL schemes we considered. This shows the possibility of describing the forward-jet cross section using the BFKL formalism at next-to-leading logarithmic accuracy. The fits using statistical errors only (which assume implicitly that the systematics are maximally correlated which is close to reality) bring about more constraints and show interesting features. The S4 fit can describe the data better ($\chi^2 = 10.0/5\text{d.o.f.}$), whereas the S3 scheme shows a higher value of χ^2 ($\chi^2 = 29.5/5$). This indicates that the S4 scheme is favored.

The curves corresponding to the fit with statistical errors only are displayed in Fig. 3 (upper plot), and they are compared with the LL-BFKL results taken from [17]. We notice the tiny difference between the LL and NLL results (the corresponding curves are barely distinguishable in the figure). This confirms that the data are consistent with the BFKL enhancement towards small values of x. Contrary to the proton structure function F_2, the forward-jet cross section $\mathrm{d}\sigma/\mathrm{d}x$ does not show large NLL-BFKL corrections, once the overall normalization fitted. This is due to the rather small value of the coupling $\bar{\alpha} \simeq 0.16$ obtained in the LL-BFKL fit [17], corresponding to an unphysically large effective scale.

We also present in Fig. 3 the fixed order QCD calculation based on the DGLAP evolution of parton densities. The next-to-leading order (NLO) prediction of forward-jet cross sections is obtained using the NLOJET++ generator [35]. CTEQ6.1M [36] parton densities were used, and the renormalization μ_{r} and the factorization scale μ_{f} were

Table 1. Results of the NLL-BFKL fits to the H1 $\mathrm{d}\sigma/\mathrm{d}x$ data. The relative values between the different overall normalizations N can be compared

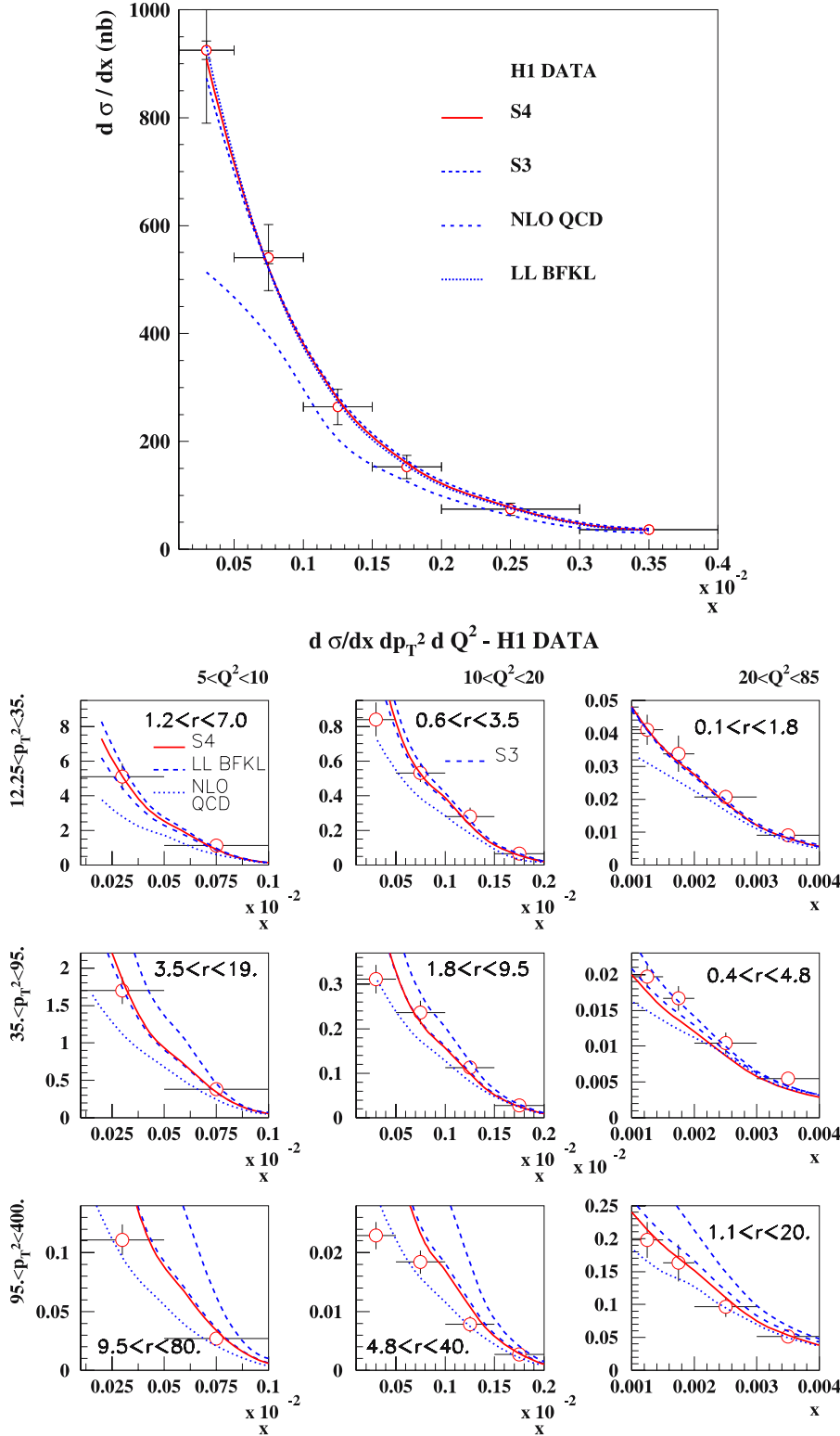| Scheme	Fit	$\chi^2/d.o.f.$	N
S3	stat. + syst.	1.15/5	1.591 ± 0.089
S3	stat. only	29.5/5	$1.640 \pm 0.019 \pm 0.204$
S4	stat. + syst.	0.48/5	1.356 ± 0.076
S4	stat. only	10.0/5	$1.374 \pm 0.016 \pm 0.172$

Fig. 3. The forward-jet cross sections $d\sigma/dx$ (*upper plot*) and $d\sigma/dx\,dQ^2\,dk_T^2$ (*lower plot*, in nb/GeV^4) measured by the H1 collaboration. Comparison with the two NLL-BFKL parametrizations S4 and S3 using the $k_T Q$ scale, and with the LL-BFKL and NLOQCD predictions. In the case of $d\sigma/dx$, we see a good agreement between the data and the BFKL fits (the NLL-BFKL fits and the LL-BFKL fit are barely distinguishable on the figure) while the NLOQCD predictions do not describe the data. For $d\sigma/dxdQ^2\,dk_T^2$, the best description of the data over the whole kinematic range is obtained in the NLL-BFKL approach

set equal to $\mu_r^2 = \mu_f^2 = Qk_T^{max}$, where k_T^{max} corresponds to the maximal transverse momentum of forward jets in the event. The NLOQCD predictions do not describe the data at small values of x, as they are lower by a factor of order 2. The sensitivity of these predictions to variations of the renormalization and factorization scales will be discussed in Sect. 6, as well as their dependence when using other parton densities.

The fit parameters obtained with statistical error only will be used in the following to make predictions for other observables, namely the triple differential cross section $d\sigma/dx\,dk_T^2\,dQ^2$. The value of $\bar{\alpha}$ for the LL-BFKL fit will

be kept as well as the normalizations of the different NLL-BFKL calculations (S3 and S4).

3.2 The triple differential cross section $\mathrm{d}\sigma/\mathrm{d}x\mathrm{d}k_\mathrm{T}^2\mathrm{d}Q^2$

The triple differential cross section $\mathrm{d}\sigma/\mathrm{d}x\,\mathrm{d}k_\mathrm{T}^2\,\mathrm{d}Q^2$ is an interesting observable as it has been measured with three different k_T^2 and Q^2 cuts, yielding nine different regions for the ratio $r = k_\mathrm{T}^2/Q^2$. It was noticed in [17] that the

LL-BFKL formalism leads to a good description of the data when r is close to 1 and deviates from the data when r is away from 1, as effects due to the ordering between Q and k_T start to set in. NLOQCD predictions show the reverse trend.

The H1 data for $\mathrm{d}\sigma/\mathrm{d}x\,\mathrm{d}k_\mathrm{T}^2\,\mathrm{d}Q^2$ are shown in Fig. 3 (lower plot), and they are compared with the S4 and S3 predictions, the LL-BFKL results (taken directly from [17]) and NLOQCD calculations. It is quite remarkable that the NLL-BFKL calculation, which includes some ordering between Q and k_T, leads to a good description of the H1
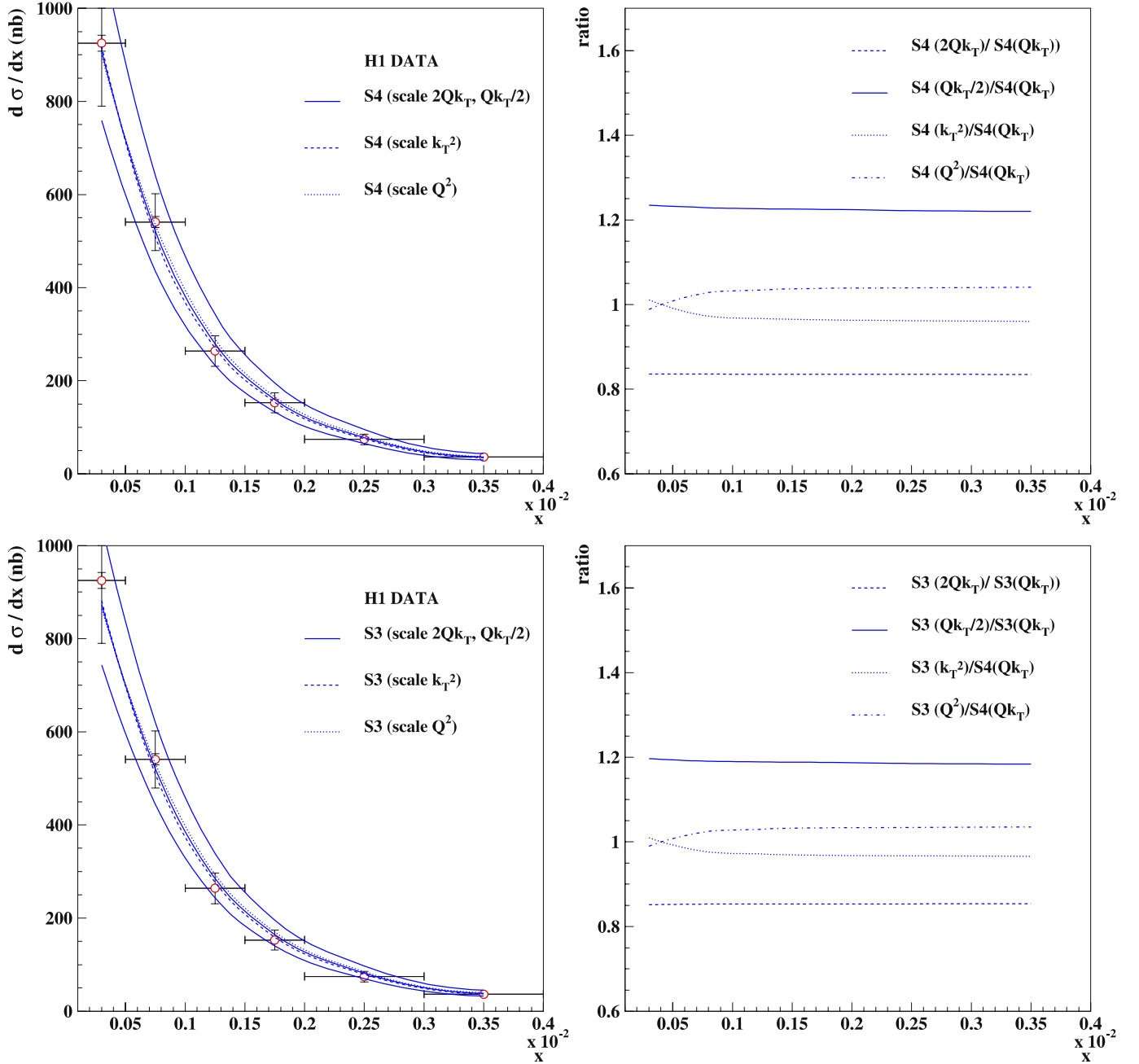

Fig. 4. Renormalization scale dependence for the $\mathrm{d}\sigma/\mathrm{d}x$ cross section. *Upper plots*: S3 scheme, *lower plots*: S4 scheme. The *left plots* show the results of the $2k_\mathrm{T}Q$ and $k_\mathrm{T}Q/2$ scales. The *right plots* show that in the considered range of renormalization scale, deviations from the scale $k_\mathrm{T}Q$ essentially affect the overall normalization. Therefore the quality of the fits (which only adjust the normalization) discussed in Sect. 3 is not altered by renormalization scale uncertainties

data over the full range. As was the case for $\mathrm{d}\sigma/\mathrm{d}x$, the difference between the LL and NLL results is small when $r \sim 1$. By contrast, when r differs from 1, the difference is significant, and the observable $\mathrm{d}\sigma/\mathrm{d}x\,\mathrm{d}k_\mathrm{T}^2\,\mathrm{d}Q^2$ is quite sensitive to NLL-BFKL effects. As a result, the best overall description of the data is obtained with the NLL-BFKL formalism.

4 Renormalization-scale dependence of the NLL description

In this section, we study the renormalization-scale dependence of the NLL-BFKL description. In the previous section, the choice was $k^2 = k_\mathrm{T}Q$ and we now test the sensitivity of our results when using $k^2 = \lambda k_\mathrm{T}Q$ with $\lambda = 2$, $\lambda = 1/2$, $\lambda = k_\mathrm{T}/Q$, or $\lambda = (Q/k_\mathrm{T})$. We use (2) with the appropriate substitution [37],

$$\bar{\alpha}(k_\mathrm{T}Q) \to \bar{\alpha}(\lambda k_\mathrm{T}Q) + b\,\bar{\alpha}^2(k_\mathrm{T}Q)\log(\lambda)\,, \qquad (11)$$

and with the effective kernel modified accordingly following (5). We also modify the energy scale $k_\mathrm{T}Q \to \lambda k_\mathrm{T}Q$.

Table 2. Impact on the fits to the H1 $\mathrm{d}\sigma/\mathrm{d}x$ data for the S4 scheme when using different renormalization scales (*upper table*) or modified impact factors (*lower table*)

Scheme	Scale	χ^2/d.o.f.	N
S4	$k_\mathrm{T}Q$	10.0/5	1.374 ± 0.016
	$2k_\mathrm{T}Q$	9.8/5	1.644 ± 0.019
	$k_\mathrm{T}Q/2$	8.8/5	1.118 ± 0.013

Scheme	Impact factor	χ^2/d.o.f.	N
S4	$\phi^\gamma(\gamma)$	10.0/5	1.374 ± 0.016
	$\phi^\gamma(1/2)$	82.6/5	0.655 ± 0.008
	$\phi_{egk}^\gamma(\gamma,\omega)$	23.0/5	2.694 ± 0.038

We first study the case of $\mathrm{d}\sigma/\mathrm{d}x$ and the results for the S3 and S4 schemes are shown in Fig. 4. We also display the results in terms of ratios with the prediction of the $k_\mathrm{T}Q$ scale chosen as the reference. We notice that the change of scale essentially affects the overall normalization and thus does not alter the quality of the fit, after readjusting the normalization. This is confirmed by the results of Table 2
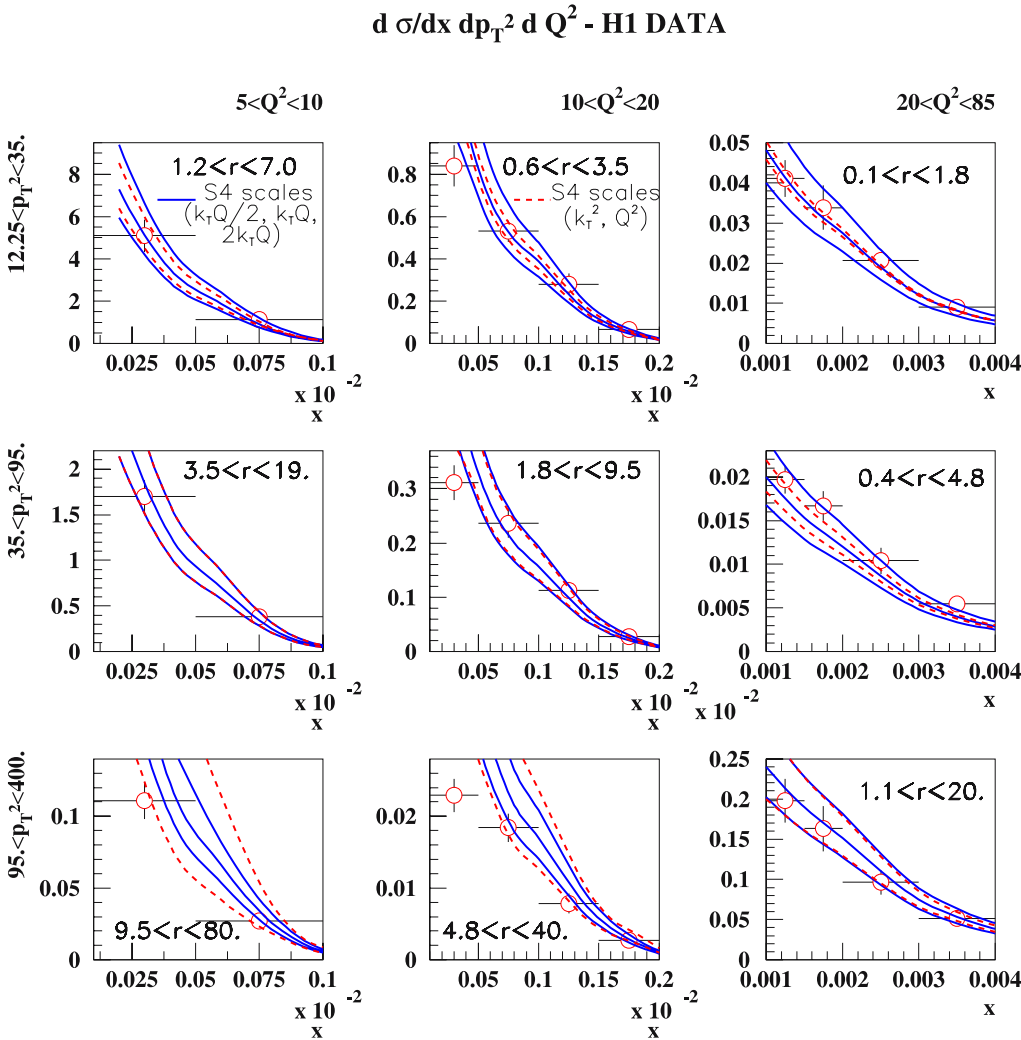

d σ/dx dp$_\mathrm{T}^2$ d Q^2 - H1 DATA

Fig. 5. Renormalization-scale dependence of the triple differential cross section $\mathrm{d}\sigma/\mathrm{d}x\,\mathrm{d}k_\mathrm{T}^2\,\mathrm{d}Q^2$ (in nb/GeV^4) for the S4 scheme

(upper table), which presents new fits performed to the $d\sigma/dx$ data for the two scales $2\,k_T Q$ and $k_T Q/2$: for each scheme, the χ^2 values are almost insensitive to the scale. Note that, for larger values of λ such as $\lambda = 4$, the quality of the fit deteriorates due to the large values reached by $\bar{\alpha}$ in the non-perturbative range. Finally, due to the cut $0.5 < k_T^2/Q^2 < 5$ used for the measurement [12], using the scales k_T^2 or Q^2 (instead of $k_T Q$) yields much less modifications and changes in χ^2.

The next step is to study the effect of the renormalization-scale dependence on the triple differential cross section. Applying the normalizations of Table 2 while computing the corresponding predictions gives, for either scale, results quite similar to those of Fig. 3. In Fig. 5, we rather show the predictions of the S4 scheme with the common normalization of Table 1, and the scale dependence is generally found to be small. The biggest effects are uncertainties of about the same magnitude as the experimental errors, and they are obtained for large values of $r = k_T^2/Q^2$. The conclusion is identical in the case of the S3 scheme.

5 Impact factor dependence of the NLL description

In this section, we study the dependence of our results on typical next-to-leading modifications of the impact factors. Indeed, since the next-to-leading impact factors are unknown, it is useful to see if our results are stable for different possible modifications. From (1) and (2) one notes that the impact factors are involved in the computation of

the fully differential cross section via the following factor in the integrand:

$$(1 - y + y^2/2)\phi_T^\gamma(\gamma) + (1-y)\phi_L^\gamma(\gamma)\,. \qquad (12)$$

In the previous section, the impact factors ϕ_T^γ and ϕ_L^γ were computed as functions of γ, and we treated unknown NLO corrections as a constant parameter. We now test the sensitivity of our results when using other prescriptions.

Our first choice is to compute the LO impact factors at $\gamma = 1/2$ and factor them out of the γ integration as well. Another prescription that we shall study is the following: implement the higher-order corrections into the impact factor that are due to the exact gluon kinematics in the $\gamma^* \to q\bar{q}g$ transition. These have been calculated in [38] and can be taken into account in our approach: this is done using the ω-dependent Mellin-transformed impact factors $\phi_{egk}^\gamma(\gamma, \omega)$, where we recall that ω is the Mellin variable conjugate to W^2/Qk_T. Denoting $\delta = \omega - 2\gamma + 1$, one writes

$$\begin{pmatrix} \phi_T^\gamma(\gamma, \omega) \\ \phi_L^\gamma(\gamma, \omega) \end{pmatrix} = \pi\alpha_{\rm em}N_c^2 \sum_q e_q^2 \frac{1}{4\gamma^2} \frac{\Gamma(\gamma+\delta)\Gamma(\gamma)}{\Gamma(\omega)(4-\delta^2)(\delta^2-1)}$$
$$\times \left[\begin{pmatrix} 3(\omega+1)^2 + \delta^2 + 8 \\ 24(\gamma+\delta)\gamma \end{pmatrix} - \frac{\psi(\gamma+\delta) - \psi(\gamma)}{2\omega\delta} \right.$$
$$\left. \times \begin{pmatrix} \omega^2[3(\omega+1)^2+9] + (\delta^2-1)(\delta^2-2\omega-9) \\ 8(\gamma+\delta)\gamma(3\omega^2-\delta^2+1) \end{pmatrix} \right]. \quad (13)$$

In practice, following (6), these impact factors are evaluated at $\omega = \bar{\alpha}(k_T Q)\chi_{\rm eff}[\gamma, \bar{\alpha}(k_T Q)]$ prior to the γ integration. This prescription is motivated by the fact that, in the
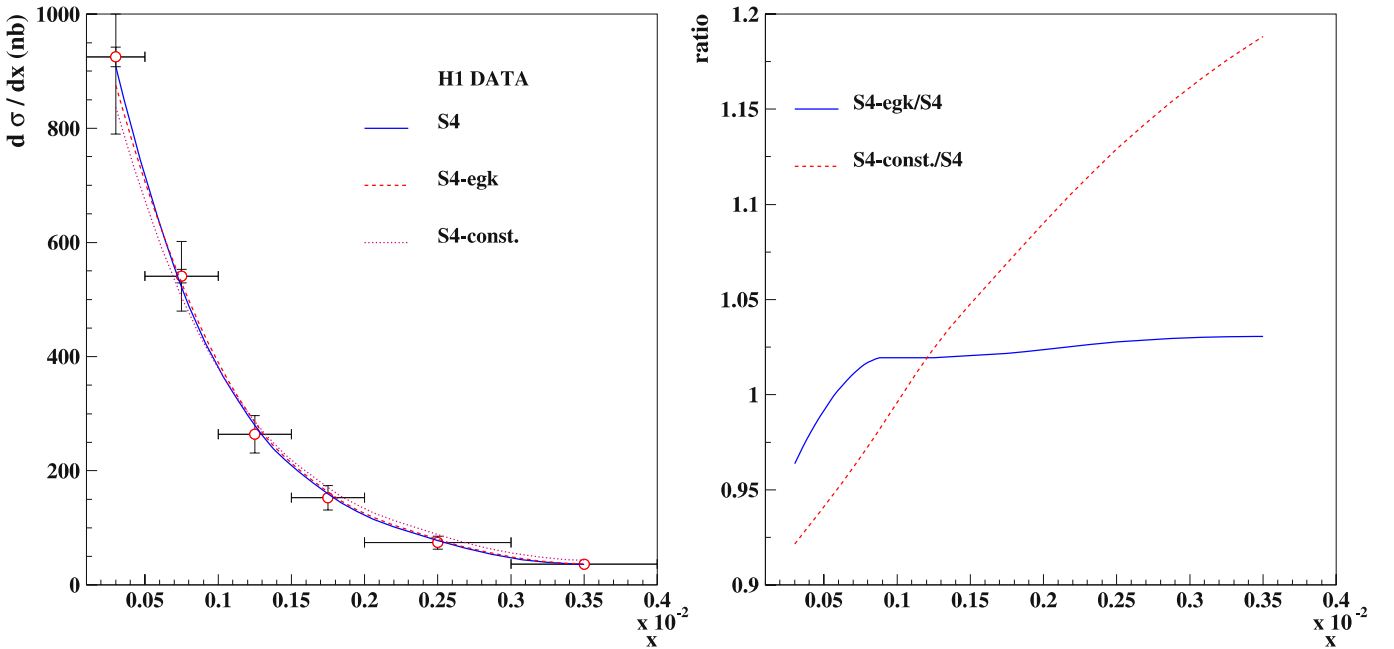

Fig. 6. Impact factor dependence for the $d\sigma/dx$ cross section in the S4 scheme. The *left plot* shows the results of the fits. The *right plot* shows that in the exact-gluon-kinematics case, the change of impact factors essentially affects the overall normalization, except at very small x, and thus modifies only slightly the quality of the fit. By contrast in the $\phi^\gamma(1/2)$ case, the χ^2 values are sensitive to modifications of the impact factor
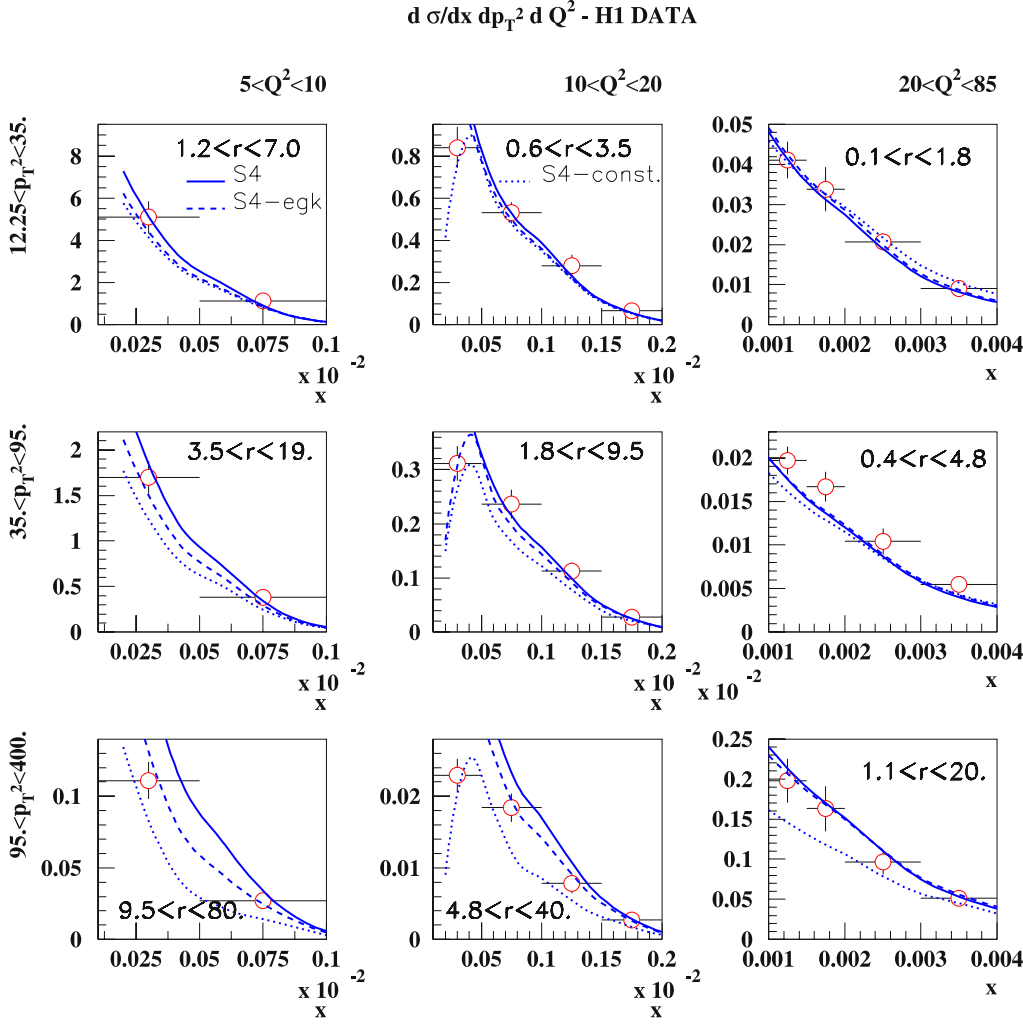
d σ/dx dp$_T$^{2} d Q^2 - H1 DATA

Fig. 7. Impact factor dependence of the triple differential cross section $\mathrm{d}\sigma/\mathrm{d}x\,\mathrm{d}k_{\mathrm{T}}^2\,\mathrm{d}Q^2$ (in nb/GeV^4) in the S4 scheme. The relative normalizations coming from the $\mathrm{d}\sigma/\mathrm{d}x$ fits have been applied

proton structure function analysis, these higher-order corrections allow for an improved DGLAP analysis [39,40]: indeed, they match the fixed-order results (at NLO and NNLO) for the splitting and coefficient functions of the DGLAP approach.

We first study the case of $\mathrm{d}\sigma/\mathrm{d}x$. Table 2 (lower table) presents new fits performed to the $\mathrm{d}\sigma/\mathrm{d}x$ data for the different prescriptions. The fit results are shown in Fig. 6 (left plot) and we also display them in terms of ratios with the prediction of the $\phi^\gamma(\gamma)$ case chosen as the reference (right plot). In the $\phi^\gamma_{egk}(\gamma,\omega)$ case, we notice that the change of impact factors essentially affects the overall normalization, except at very small values of x, where the gluon kinematics become more restrictive. As a result the quality of the fit, which readjusts the normalization, is only slightly modified. By contrast in the $\phi^\gamma(1/2)$ case, the shape is clearly different, which yields a bad χ^2.

After applying the normalizations of Table 2 (lower table), we now compare the effect of the different impact factors on the triple differential cross section. The results are given in Fig. 7. The effect is found to be small in the exact-gluon kinematics case and even slightly improves the description. By contrast, differences are important in the $\phi^\gamma(1/2)$ case, especially at large values of $r = k_{\mathrm{T}}^2/Q^2$.

6 PDF and scale dependence of the NLOQCD predictions

To obtain the NLOQCD predictions of the forward-jet data, the photon–parton hard cross section is computed at next-to-leading order in α_s, and the leading and next-to-leading logarithms $\alpha_s^n \log^n Q^2$ and $\alpha_s^n \log^{n-1} Q^2$ are resummed using the DGLAP equations [5–8], which govern the evolution of the parton distribution functions (PDFs) of the proton.

The prediction for the forward-jet cross section at next-to-leading order is calculated using NLOJET++ [35]. The renormalization scale μ_{r}^2 and the factorization scale μ_{f}^2 were chosen as $\mu_{\mathrm{r}}^2 = \mu_{\mathrm{f}}^2 = Qk_{\mathrm{T}}^{\mathrm{max}}$, where $k_{\mathrm{T}}^{\mathrm{max}}$ denotes the maximal transverse momentum of forward jets in the event. To obtain the uncertainty associated with the choice of the scale, we varied the scales in the conventional range $Qk_{\mathrm{T}}^{\mathrm{max}}/4 < \mu_{\mathrm{r}}^2 = \mu_{\mathrm{f}}^2 < 4Qk_{\mathrm{T}}^{\mathrm{max}}$. Another scale choice, $\mu_{\mathrm{r}}^2 = \mu_{\mathrm{f}}^2 = k_{\mathrm{T}}^{\mathrm{max}2}$ was also tested; however, it yielded a result located within the mentioned scale uncertainty bounds and thus shall not be considered further. We point out that the scale uncertainty is rather large in the low-x regime. This is due to the large NLO cor-

rection suggesting that higher-order corrections might be significant.

An additional contribution to the total uncertainty of the calculation is due to the choice of the PDFs of the proton. Throughout the calculation, we use the CTEQ6.1M PDF parametrization, which provides not only the central PDF S_0 corresponding to the best fit to data, but also

40 additional distribution functions S_i^+, S_i^-, $i = 1 \ldots 20$ devoted to uncertainty studies [36]. The total PDF uncertainty ΔX of the observable X is then computed as

$$(\Delta X)^2 = \sum_{i=1}^{20} \left[\frac{X(S_i^+) - X(S_i^-)}{2} \right]^2 . \qquad (14)$$
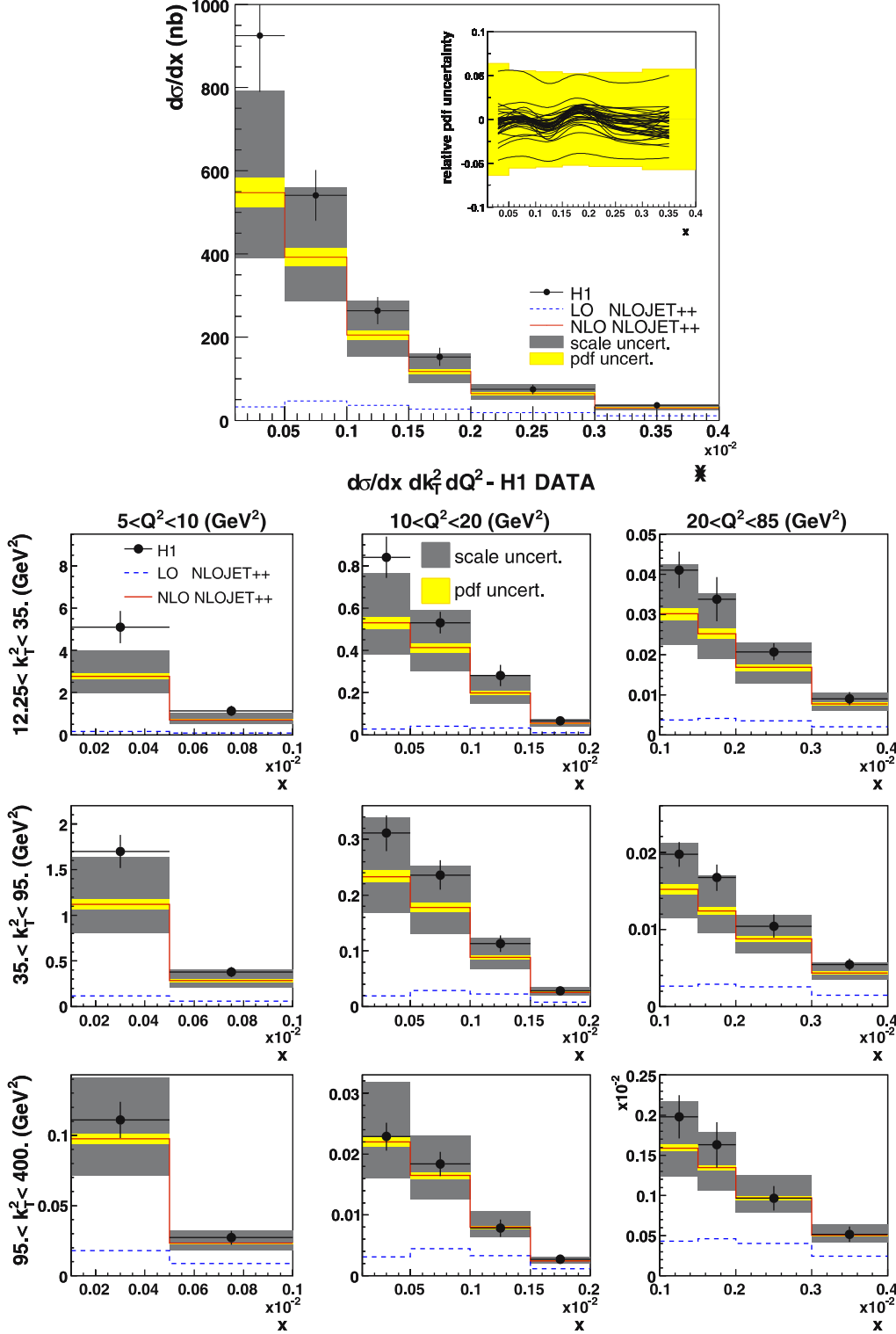

Fig. 8. *Upper plot*: scale and PDF uncertainties of the dσ/dx distribution; the particular contributions of 40 different PDFs from CTEQ6.1M to the total PDF uncertainty (*yellow area*) is depicted in the inset. *Lower plot*: scale and PDF uncertainties for the triple differential distribution dσ/dxdQ^2dk_T^2 (in nb/GeV^4). In both cases, the scales varying in the range $0.25 \ Qk_T^{\max} < \mu_r^2 = \mu_f^2 < 4 \ Qk_T^{\max}$ are displayed (*shaded gray area*)

We noticed that the main contribution to the PDF uncertainty comes from the gluon PDF.

The DGLAP calculation of the $\mathrm{d}\sigma/\mathrm{d}x$ distribution measured by H1 is presented in Fig. 8, upper plot. This approach clearly fails to describe the data for the low values of x. In comparison with Fig. 3, we see that $\mathrm{d}\sigma/\mathrm{d}x$ is more sensitive to the BFKL dynamics than the triple differential distribution, as the deviation from the data is obvious.

The PDF uncertainty study is shown in the inset. The solid lines represent the ratio of the cross section calculated with the various PDFs S_i^+, S_i^-, normalized to the cross section calculated with the central PDF S_0. The gluon PDF ($i=15$) has the greatest impact on the uncertainty and the other PDFs can be neglected. The uncertainty study of $\mathrm{d}\sigma/\mathrm{d}x\,\mathrm{d}k_\mathrm{T}^2\,\mathrm{d}Q^2$ is shown in Fig. 8, lower plot. The PDF uncertainty was obtained taking into account the gluon density (which practically dictates the overall PDF uncertainty) only.

The main conclusion that can be drawn from Fig. 8 is that at low values of x, the NLOQCD results suffer from large uncertainties, and they indicate that NNLO calculations are needed to obtain genuine predictions in this framework.

7 Conclusions

We performed a phenomenological analysis of the H1 forward-jet data, looking for effects of next-to-leading logarithms in the BFKL approach. Let us briefly summarize our results.

- For the cross section $\mathrm{d}\sigma/\mathrm{d}x$, measured in the kinematical regime $Q^2/k_\mathrm{T}^2 \sim 1$, we obtain a good description of the H1 data by NLL-BFKL predictions (see Table 1 and Fig. 3, upper plot). In addition, the difference between the LL-BFKL and NLL-BFKL descriptions is very small once the overall normalization is fit. This confirms the validity of the BFKL description of [16, 17] previously obtained with the LL formula and a rather small effective coupling.
- In the case of the triple differential cross section $\mathrm{d}\sigma/\mathrm{d}x\,\mathrm{d}k_\mathrm{T}^2\,\mathrm{d}Q^2$, the same conclusions holds when $r = k_\mathrm{T}^2/Q^2 \sim 1$. In addition when r differs from 1, the NLL-BFKL description is quite different from the LL-BFKL one, as it is closer to the NLOQCD calculation. As a result, the best overall description of the data for $\mathrm{d}\sigma/\mathrm{d}x\,\mathrm{d}k_\mathrm{T}^2\,\mathrm{d}Q^2$ is obtained with the NLL-BFKL formalism (see Fig. 3, lower plot).
- The renormalization-scale dependence of our results has been thoroughly studied and we showed the stability of the NLL-BFKL approach when using the scales $k_\mathrm{T}Q$, $2k_\mathrm{T}Q$ and $k_\mathrm{T}Q/2$. For $\mathrm{d}\sigma/\mathrm{d}x$, the change of scale essentially affects the overall normalization and does not alter the quality of the fits (see Fig. 4 and Table 2, upper table). For $\mathrm{d}\sigma/\mathrm{d}x\,\mathrm{d}k_\mathrm{T}^2\,\mathrm{d}Q^2$, the biggest effect yields an uncertainty of about the same magnitude as the experimental errors (see Fig. 5).
- We want to stress that the HERA data allow for a detailed study of the NLL-BFKL approach and of the QCD dynamics of forward jets. In particular, it has the potential to address the question of the remaining ambiguity corresponding to the dependence on the specific regularization scheme of the NLL kernel. For instance, the predictions of the S3 scheme do not compare with the data as well as the predictions of the S4 scheme, as indicated by the χ^2 values given in Table 1. Therefore, it would be very interesting to compare the data with other regularization procedures [22–24, 37] than those used here. However, these other solutions proposed to remove the spurious singularities of the NLL kernel are not in such a suitable form for phenomenology; hence this issue will be addressed in a separate work.
- Our analysis is to be completed with the next-to-leading photon impact factors, when available. However, we tested the stability of our approach when implementing typical next-to-leading modifications of leading-order impact factors. The results show some sensitivity (see Figs. 6, 7 and Table 2, lower table) with the $\phi^\gamma(1/2)$ prescription. It is, however, interesting that using the impact factors (13) with exact gluon kinematics (which, in the structure function case, allow for an improved DGLAP analysis) still gives a good fit of the $\mathrm{d}\sigma/\mathrm{d}x$ data and also a better description of the $\mathrm{d}\sigma/\mathrm{d}x\,\mathrm{d}k_\mathrm{T}^2\,\mathrm{d}Q^2$ cross section. This indicates that, when the next-to-leading impact factors will be known, our predictions could be stable.
- Finally, we computed the NLOQCD predictions using the NLOJET++ generator and CTEQ6.1M [36] parton densities. We tested their relevance by comparing the use of different parton densities and renormalization and factorization scales (see Fig. 8). The NLOQCD predictions do not describe the data at small values of x, and they suffer from large uncertainties, showing the need for higher-order corrections in this framework.

Forward-jet production is the first observable for which the NLL-BFKL description works, while the standard NLOQCD does not work. We need complete knowledge of the next-to-leading impact factors before drawing final conclusions, but our analysis strongly suggests that the data show the BFKL enhancement at small values of x. This is of great interest in view of the LHC, where similar QCD dynamics will be tested with Mueller–Navelet jets [41–45].

Appendix A: The S3 and S4 regularization schemes

In this appendix, we recall the regularization procedure of [19] to obtain $\chi_{\mathrm{NLL}}(\gamma, \omega)$ in the S3 and S4 schemes. The starting point is the scale invariant (and $\gamma \leftrightarrow 1 - \gamma$ symmetric) part of the NLL-BFKL kernel

$$\chi_1(\gamma) = \frac{3}{2}\zeta(3) + \left(\frac{1+5b}{3} - \frac{\zeta(2)}{2}\right)\chi_{\mathrm{LL}}(\gamma) - \frac{b}{2}\chi_{\mathrm{LL}}^2(\gamma)$$

$$+ \frac{1}{4} \left[\psi''(\gamma) + \psi''(1-\gamma) \right]$$

$$- \phi(\gamma) - \frac{\pi^2 \cos(\pi\gamma)}{4 \sin^2(\pi\gamma)(1-2\gamma)}$$

$$\times \left[3 + \left(1 + \frac{N_f}{N_c^3} \right) \frac{2+3\gamma(1-\gamma)}{(3-2\gamma)(1+2\gamma)} \right], \quad \text{(A.A.1)}$$

with b given in (3), χ_{LL} given in (9), and

$$\phi(\gamma)$$

$$= \frac{1}{2} \sum_{k=0}^{\infty} \frac{k+1/2}{(k+\gamma)(k+1-\gamma)} \left[\psi'\left(\frac{k+2}{2}\right) - \psi'\left(\frac{k+1}{2}\right) \right].$$

(A.A.2)

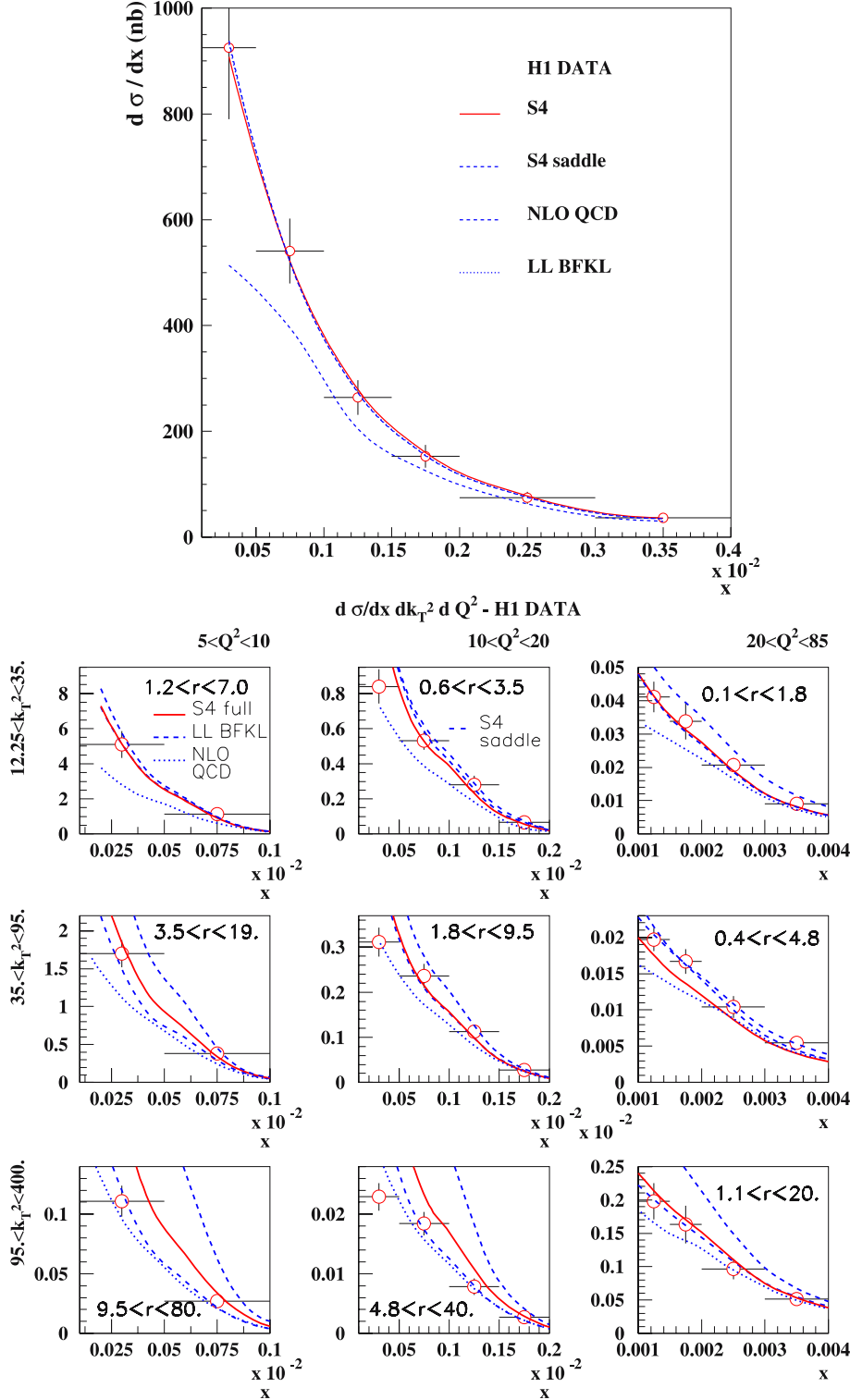**Fig. 9.** The forward-jet cross sections $\mathrm{d}\sigma/\mathrm{d}x$ (*upper plot*) and $\mathrm{d}\sigma/\mathrm{d}x\,\mathrm{d}Q^2\,\mathrm{d}k_{\mathrm{T}}^2$ (*lower plot*, in nb/GeV^4) measured by the H1 collaboration and compared with two NLL-BFKL predictions of the S4 scheme, obtained with the exact γ integration (2) or the saddle-point approximation (B.B.2). The LL-BFKL and NLOQCD results are also recalled

The pole structure of $\chi_1(\gamma)$ at $\gamma = 0$ (and by symmetry at $\gamma = 1$) is

$$\chi_1(\gamma) = -\frac{1}{2\gamma^3} + \frac{d_2}{\gamma^2} + \frac{d_1}{\gamma} + \mathcal{O}(1), \qquad \text{(A.A.3)}$$

with

$$d_1 = -\frac{N_f}{18N_c}\left(5 + \frac{13}{2N_c^2}\right), \quad d_2 = -\frac{11}{8} + \frac{N_f}{12N_c}\left(1 - \frac{2}{N_c^2}\right). \qquad \text{(A.A.4)}$$

The S3 scheme kernel $\chi_{S3}(\gamma, \omega)$ is given by

$$\chi_{S3}(\gamma, \omega) = [1 - \bar{\alpha}A]$$
$$\times \left[2\psi(1) - \psi\left(\gamma + \frac{2\bar{\alpha}B + \omega}{2}\right) - \psi\left(1 - \gamma + \frac{2\bar{\alpha}B + \omega}{2}\right)\right]$$
$$+ \bar{\alpha}\left\{\chi_1(\gamma) + A\chi_{LL}(\gamma) + \left(B + \frac{\chi_{LL}(\gamma)}{2}\right)\right.$$
$$\left. [\psi'(\gamma) + \psi'(1 - \gamma)]\right\}, \qquad \text{(A.A.5)}$$

with A and B chosen to cancel the singularities of $\chi_1(\gamma)$ at $\gamma = 0$: $A = -d_1 - \pi^2/6$ and $B = -d_2$.

The S4 scheme kernel $\chi_{S4}(\gamma, \omega)$ is defined with the help of the function $f(\gamma) = 1/\gamma + 1/(1 - \gamma)$:

$$\chi_{S4}(\gamma, \omega) = \chi_{LL}(\gamma) - f(\gamma) + [1 - \bar{\alpha}A]f(\omega + 2\bar{\alpha}B, \gamma)$$
$$+ \bar{\alpha}\left\{\chi_1(\gamma) + Af(\gamma)\right.$$
$$\left. + \left(B + \frac{\chi_{LL}(\gamma)}{2}\right)\left[\frac{1}{\gamma^2} + \frac{1}{(1 - \gamma)^2}\right]\right\}. \qquad \text{(A.A.6)}$$

In this scheme, A and B are given by $A = -d_1 - 1/2$ and $B = -d_2$.

Appendix B: Comparison between the exact NLL-BFKL γ integration and a saddle-point approximation

It is possible to estimate the complex integration in (2) using a saddle-point approximation in γ. In the BFKL regime we are working in, Y is very large, and the saddle-point equation

$$\frac{d\chi_{\text{eff}}}{d\gamma}(\gamma_c, \bar{\alpha}) = \chi'_{\text{eff}}(\gamma_c, \bar{\alpha}) = \frac{\log(k_T^2/Q^2)}{\bar{\alpha}Y} \qquad \text{(B.B.1)}$$

becomes $\chi'_{\text{eff}}(\gamma_c, \bar{\alpha}) = 0$. Hence one finds for the theoretical forward-jet cross section

$$\frac{d\sigma_{T,L}^{\gamma^* p \to JX}}{dx_J\, dk_T^2} \simeq \frac{\alpha_s(k_T^2)\alpha_s(Q^2)}{k_T^2 Q^2} f_{\text{eff}}(x_J, k_T^2)\left(\frac{Q^2}{k_T^2}\right)^{\gamma_c}$$
$$\times \frac{\phi_{T,L}^\gamma(\gamma_c)}{\sqrt{2\pi\bar{\alpha}\chi''_{\text{eff}}(\gamma_c, \bar{\alpha})\, Y}}$$
$$\times \exp\left(\bar{\alpha}\chi_{\text{eff}}(\gamma_c, \bar{\alpha})Y - \frac{\log^2(Q^2/k_T^2)}{2\bar{\alpha}\chi''_{\text{eff}}(\gamma_c, \bar{\alpha})Y}\right), \qquad \text{(B.B.2)}$$

where $\chi''_{\text{eff}} = d^2\chi_{\text{eff}}/d\gamma^2$.

For each set of scales (Q^2, k_T^2), it is possible to extract the values of γ_c, $\bar{\alpha}\chi_{\text{eff}}(\gamma_c, \bar{\alpha})$ and $\bar{\alpha}\chi''_{\text{eff}}(\gamma_c, \bar{\alpha})$ after solving the implicit equation (5).

This approach was considered in [29] and compared with the results obtained with the exact integration. In this appendix we discuss this comparison in more detail. At the level of the differential cross sections (2) and (B.B.2) there are some differences between the exact NLL-BFKL integration and the saddle-point approximation. But when considering the integrated, experimentally measured cross sections $d\sigma/dx$ and $d\sigma/dx\,dk_T^2\,dQ^2$, the description of the data is similar. This is shown in Fig. 9.

We recall that, starting from (1), one has to carry out a number of integrations over the kinematic variables, which have to be done while properly taking into account the kinematic cuts applied for the different measurements [17]. This procedure seems to erase the differences between the exact NLL-BFKL integration and the saddle-point approximation. This is even more so for $d\sigma/dx$.

References

1. A.H. Mueller, J. Phys. G **17**, 1443 (1991)
2. L.N. Lipatov, Sov. J. Nucl. Phys. **23**, 338 (1976)
3. E.A. Kuraev, L.N. Lipatov, V.S. Fadin, Sov. Phys. JETP **45**, 199 (1977)
4. I.I. Balitsky, L.N. Lipatov, Sov. J. Nucl. Phys. **28**, 822 (1978)
5. G. Altarelli, G. Parisi, Nucl. Phys. B **126**, 298 (1977)
6. V.N. Gribov, L.N. Lipatov, Sov. J. Nucl. Phys. **15**, 438 (1972)
7. V.N. Gribov, L.N. Lipatov, Sov. J. Nucl. Phys. **15**, 675 (1972)
8. Y.L. Dokshitzer, Sov. Phys. JETP **46**, 641 (1977)
9. V.S. Fadin, L.N. Lipatov, Phys. Lett. B **429**, 127 (1998)
10. M. Ciafaloni, Phys. Lett. B **429**, 363 (1998)
11. M. Ciafaloni, G. Camici, Phys. Lett. B **430**, 349 (1998)
12. H1 Collaboration, A. Aktas et al., Eur. Phys. J. C **46**, 27 (2006)
13. ZEUS Collaboration, S. Chekanov et al., Phys. Lett. B **632**, 13 (2006)
14. H1 Collaboration, C. Adloff et al., Nucl. Phys. B **538**, 3 (1999)
15. ZEUS Collaboration, J. Breitweg et al., Eur. Phys. J. C **6**, 239 (1999)
16. J.G. Contreras, R. Peschanski, C. Royon, Phys. Rev. D **62**, 034006 (2000)
17. C. Marquet, C. Royon, Nucl. Phys. B **739**, 131 (2006)
18. H. Jung, L. Jonsson, H. Kuster, Eur. Phys. J. C **9**, 383 (1999)
19. G.P. Salam, JHEP **9807**, 019 (1998)
20. M. Ciafaloni, D. Colferai, G.P. Salam, Phys. Rev. D **60**, 114036 (1999)
21. M. Ciafaloni, D. Colferai, G.P. Salam, JHEP **9910**, 017 (1999)
22. S.J. Brodsky, V.S. Fadin, V.T. Kim, L.N. Lipatov, G.B. Pivovarov, JETP Lett. **70**, 155 (1999)
23. R.S. Thorne, Phys. Rev. D **60**, 054031 (1999)
24. G. Altarelli, R.D. Ball, S. Forte, Nucl. Phys. B **621**, 359 (2002)

25. J. Bartels, D. Colferai, S. Gieseke, A. Kyrieleis, Phys. Rev. D **66**, 094 017 (2002)
26. V.S. Fadin, D.Y. Ivanov, M.I. Kotsky, Nucl. Phys. B **658**, 156 (2003)
27. J. Bartels, A. Kyrieleis, Phys. Rev. D **70**, 114 003 (2004)
28. R. Peschanski, C. Royon, L. Schoeffel, Nucl. Phys. B **716**, 401 (2005)
29. O. Kepka, C. Marquet, R. Peschanski, C. Royon, Phys. Lett. B **655**, 236 (2007)
30. J. Kwiecinski, A.D. Martin, P.J. Sutton, Z. Phys. C **71**, 585 (1996)
31. B. Andersson, G. Gustafson, H. Kharraziha, J. Samuelsson, Z. Phys. C **71**, 613 (1996)
32. Y.V. Kovchegov, A.H. Mueller, Phys. Lett. B **439**, 428 (1998)
33. J. Bartels, D. Colferai, G.P. Vacca, Eur. Phys. J. C **24**, 83 (2002)
34. J. Bartels, Eur. Phys. J. C **29**, 235 (2003)
35. Z. Nagy, Z. Trocsanyi, Phys. Rev. Lett. **87**, 082 001 (2001)
36. J. Pumplin, D.R. Stump, J. Huston, H.L. Lai, P. Nadolsky, W.K. Tung, JHEP **0207**, 012 (2002)
37. M. Ciafaloni, D. Colferai, G.P. Salam, A.M. Stasto, Phys. Rev. D **68**, 114 003 (2003)
38. A. Bialas, H. Navelet, R. Peschanski, Nucl. Phys. B **603**, 218 (2001)
39. C.D. White, R.S. Thorne, Eur. Phys. J. C **45**, 179 (2006)
40. C.D. White, R. Peschanski, R.S. Thorne, Phys. Lett. B **639**, 652 (2006)
41. A.H. Mueller, H. Navelet, Nucl. Phys. B **282**, 727 (1987)
42. C. Marquet, R. Peschanski, Phys. Lett. B **587**, 201 (2004)
43. C. Marquet, R. Peschanski, C. Royon, Phys. Lett. B **599**, 236 (2004)
44. A. Sabio Vera, F. Schwennsen, Nucl. Phys. B **776**, 170 (2007)
45. C. Marquet, C. Royon, Azimuthal decorrelation of Mueller–Navelet jets at the Tevatron and the LHC. arXiv:0704.3409 [hep-ph]